Article

Relations between Geometric Parameters and Numerical Simulation Accuracy in Modeling Signal Transmission in the Presynaptic Bouton

Maciej Gierdziewicz [ID]

Faculty of Automation, Electrical Engineering, Computer Science and Biomedical Engineering,
AGH University of Science and Technology, Al. Mickiewicza 30, 30-059 Cracow, Poland; gierdzma@agh.edu.pl

Featured Application: The methodology described in this paper may be used, and will be used by the authors of this and related works, to (1) examine the influence of various factors, including the shape of the bouton and its neurotransmitter synthesis domains as well as the release sites and various organelles, on the course of the nerve impulse. And, vice versa, (2) to detect some abnormalities in the composition o the synapse basing on the shape of its electrical output.

Abstract: In order to examine nerve impulses by means of simulation methodology, the models of all parts of nervous system, well suited for numerical modeling, are needed. In this paper the problem of setting up such a model, namely, that of a presynaptic bouton, is addressed. Simulation of the neurotransmitter flow inside the presynaptic bouton is performed. The transport is modeled with a partial differential equation with an additional nonlinear term. Two ways of modeling the bouton are applied. One of them let reflect a complex shape of the bouton and of some inner organelles. The influence of the generated mesh quality on the accuracy of numerical simulations is studied by comparing the released amount of neurotransmitter. The only mesh that produced diminished output was the worst one. The conclusion is that even slightly optimized tetrahedral mesh is suitable for calculations.

Keywords: presynaptic bouton; differential diffusive model; numerical three-dimensional simulations; finite elements method; three-dimensional mesh generation; mesh quality measures

1. Introduction

Dynamical processes in the neuron [1] include, among others, those concerning the release of neurotransmitter (NT) into the synaptic cleft. The release occurs via calcium channels [2,3] and the amount of the released NT is measured indirectly by the postsynaptic potential. In Figure 1A in the cited paper [3] the connection between NT amount and postsynaptic current is illustrated; in Figure 3C in other work [4] the shape of the impulse in genetically different animals is presented; diminished amplitude means impaired genotype. The above mentioned dynamical processes are often described by using differential equations [5–7], including − for a long time − partial ones [8–10]. The equation of this type can not, usually, be solved analytically, and therefore numerical methods have to be used [10–13]. In order to perform the calculations quickly and accurately, the appropriately designed mesh, in the nodes of which the calculations will be made, should be created. In biological sciences the boundary conditions are generated by the modeled organelles in biological structure of the cell. For example, what the model should take into account is the work of the active zone of the presynaptic bouton during exocytosis. It is one of the crucial mechanisms in transmitting nerve impulses and it is accomplished by means of Ca_V2 channel (one of three kinds of similar channels: Ca_V1, Ca_V2 and Ca_V3) [4]. Therefore, the design of a good mesh is a difficult problem connected with the mesh

geometrical properties [14,15]. Tetrahedral meshes are also studied in the context of automatic adjustment [16]. Finite Elements Method, on the other hand, requires a high quality mesh [17]. This means that a single cell should be as regular as possible—an equilateral triangle in two dimensions, and in the 3D case—a regular tetrahedron. Generally, it is impossible to reach this goal in practice because of the geometric properties of the modeled object. Additionally, regular tetrahedra can not be used as elements of a spatial mesh. In reality, such tetrahedra differ in shape and size; also, the regions joining different parts of the model are usually covered with elements of worse quality.

In this paper the problem of dependence of numerics precision on the quality of the spatial data structure (a tetrahedral mesh) for numerical calculations for processes in the neuron axon terminal is studied. Various geometrical presynaptic bouton models are discussed. They are compared by using several different parameters of the quality of the mesh, one of them formerly introduced [18]. The differences in the results of simulations for different meshes, with other parameters kept unchanged, are analyzed. The adequate measure of the differences is the amount of neurotransmitter released to the synaptic cleft.

This paper is a continuation of the studies described in [6,8,11,12,18–22].

2. Model

Since the transport of neurotransmitter (NT) in the presynaptic bouton of the neuron has to be considered both in spatial and in temporal aspect, the partial differential equation model has been introduced, derived from the diffusion equation with nonlinear modifications. The more detailed description of the model is presented in [8]. Main aspects of the model are given below.

2.1. Diffusive PDE Model

When setting up the model, the following was assumed:

The presynaptic bouton occupies a bounded subset Ω of three-dimensional space. The NT supply takes places in the bouton subdomain Ω_1 (supply zone), thereby increasing the total amount of NT in the bouton. On the other hand, the release through the subset Γ_d of the bouton membrane $\partial\Omega$ decreases that amount. The NT flow in the presynaptic bouton, basing on the similar study [22], was modeled with the following partial differential Equation (1):

$$\varrho_t(x,t) = a\Delta\varrho(x,t) + f(x)(\bar{\varrho} - \varrho(x,t))^+ \quad \text{in} \quad \Omega \times (0,T), \tag{1}$$

where $\varrho(x,t)$ is the density of NT at time t and at the spatial location x and a is the diffusion coefficient. The appropriate initial conditions had to be set and, similarly, the boundary conditions [22] should be modeled by the Equation (2)

$$-\frac{\partial\varrho(x,t)}{\partial\nu} = \eta(t)\alpha\varrho(x,t) \quad \text{on} \quad \Gamma_d \times (0,T) \tag{2}$$

where α is the permeability coefficient and $\partial/\partial\nu$ is a directional derivative in the outer normal direction ν. The function $\eta(t)$ (depending on time t) takes the value of 1 for $t \in [t_n, t_n + \tau]$ (with the action potential arriving at t_n and with the release time τ), and $\eta(t) = 0$ otherwise [19]. In such a way, boundary conditions are a simple model of exocytosis through a Ca_V2 type voltage-gated channel.

When the Equation (1) is multiplied by a smooth function $v : \Omega \to \mathbb{R}$, and after integrating by parts [22], we obtain

$$\int_\Omega \varrho_t(x,t)v(x)\,dx + a\int_\Omega \nabla\varrho(x,t)\cdot\nabla v(x)\,dx \tag{3}$$

$$+ \alpha\eta(t)\int_{\Gamma_d} \varrho(x,t)v(x)\,dS = \beta\int_{\Omega_1} (\bar{\varrho} - \varrho(x,t))^+ v(x)\,dx.$$

which is valid when ϱ is sufficiently smooth.

2.2. 3D Simulations—The Finite Elements Method

Piecewise linear C^0 finite elements (tetrahedra) are used to perform the calculations according to the numerical scheme [22]. The function ϱ_h, which approximates ϱ, is calculated as

$$\varrho_h(x,t) = \sum_{i=1}^{K} \varrho_i(t)v_i(x),$$

where v_i are the basis functions of the finite elements space. When the following matrices are introduced: the mass matrix $\mathcal{G} = \{g_{ij}\}_{i,j=1}^{K}$, the stiffness matrix $\mathcal{A}_1 = \{a_{ij}^1\}_{i,j=1}^{K}$, and the release matrix $\mathcal{A}_2 = \{a_{ij}^2\}_{i,j=1}^{K}$, and when the additional assumption is made that $\mathcal{A}(t) = \mathcal{A}_1 + \eta(t)\mathcal{A}_2$, and the nonlinear operator $\mathcal{B} : \mathbb{R}^K \to \mathbb{R}^K$ is applied according to [22]:

$$\mathcal{B}(\varrho_1, \ldots, \varrho_K)_j = \beta \int_{\Omega_1} \left(\bar{\varrho} - \sum_{i=1}^{K} \varrho_i v_i(x) \right)^+ v_j(x)\, dx. \tag{4}$$

the numerical scheme may be rewritten as

$$\mathcal{G}\varrho_h'(t) + \mathcal{A}(t)\varrho_h(t) = \mathcal{B}(\varrho_h(t)).$$

The time step is defined as $t_k = k\Delta t$ where Δt is at least several times smaller than τ. After the approximation of ϱ_h^k by $\varrho_h(t_k)$, the Crank–Nicholson approximative scheme can be used

$$\mathcal{G}\frac{\varrho_h^k - \varrho_h^{k-1}}{\Delta t} + \frac{1}{2}\mathcal{A}(t_k)\varrho_h^k + \frac{1}{2}\mathcal{A}(t_{k-1})\varrho_h^{k-1} = \frac{1}{2}\mathcal{B}(\varrho_h^k) + \frac{1}{2}\mathcal{B}(\varrho_h^{k-1}), \tag{5}$$

valid for $k = 1, 2, \ldots$. In the finite element basis $\{v_k\}_{k=1}^{K}$, ϱ_0 is approximated by ϱ_h^0. The scheme must be solved for ϱ_h^k. The problem of the nonlinearity in $\mathcal{B}$ is dealt with by the iterative scheme:

$$\varrho_h^{k(0)} = \varrho_h^{k-1}, \tag{6}$$
$$\mathcal{G}\frac{\varrho_h^{k(m+1)} - \varrho_h^{k-1}}{\Delta t} + \frac{1}{2}\mathcal{A}(t_k)\varrho_h^{k(m+1)} + \frac{1}{2}\mathcal{A}(t_{k-1})\varrho_h^{k-1} = \frac{1}{2}\mathcal{B}(\varrho_h^{k(m)}) + \frac{1}{2}\mathcal{B}(\varrho_h^{k-1}),$$

in which the inner iteration step is denoted by the index m. In such a way, the scheme gives a linear system of equations for each iteration. Iterating stops when $|\varrho_h^{k(m+1)} - \varrho_h^{k(m)}|$ is sufficiently small.

For the numerical simulations, the bouton is modeled as a bounded polyhedral domain $\Omega \subset \mathbb{R}^3$. The boundary of the bouton, $\partial\Omega$, is represented by a set of flat polygons. The proper polyhedral subset of the bouton, Ω_1, is the domain of vesicles supply. The release site Γ_d is modeled as a finite sum of flat polygons.

3. Generation of the Mesh

As it has already been mentioned [18], the problem of generating a mesh of a complex object is difficult. Firstly, a reasonable compromise must be found between a mesh with a very large number of small tetrahedra (increased computing time) and another one with a small number of relatively large elements (errors in simulating flow near tiny substructures). Secondly, the mesh elements should be as regular as possible [23].

3.1. Mesh Element Quality

The mesh quality parameters, considered below and calculated for each element, are as follows.

Assuming that S denotes the total surface, and V—the total volume of the tetrahedron, the following parameters have been used [18]: The first of the defined parameters was

$$SV = \frac{\sqrt{S}}{\sqrt[3]{V}}$$

The second parameter was the ratio of the longest edge and the radius of the inscribed sphere [24]:

$$ER = \frac{l_{max}}{r_{ins}},$$

ranging from $ER_{min} = 2\sqrt{6} \approx 4.89898$, for a regular tetrahedron, to infinity.

The third one is the value applied in the TetGen program [25,26] i.e., the longest edge divided by the smallest height (EH)

$$EH = \frac{l_{max}}{h_{min}},$$

with the range similar as in the previous example i.e., from $EH_{min} = \sqrt{\frac{3}{2}} \approx 1.22474$ to infinity, following the same rule as before: "the larger the value, the worse the tetrahedron".

The last two parameters are $MAXS$ and $MINS$, and they are computed as the ratios of the largest (S_{max}) or the smallest (S_{min}) face measure, respectively, to the total surface (S) of the tetrahedron.

The formula for the first of those two parameters is

$$MAXS = \frac{S_{max}}{S}$$

and its value ranges from 0.25 to 0.5 i.e.,

$$MAXS \in [0.25; 0.5)$$

The formula for the second parameter is

$$MINS = \frac{S_{min}}{S}$$

and its value ranges from 0 to 0.25 i.e.,

$$MINS \in (0; 0.25]$$

The parameters mentioned above (SV, ER, EH, MAXS and MINS) is positive and dimensionless. All of them, except MINS, have the smallest value for the regular tetrahedron. The MINS value behaves differently: the closer to zero, the worse the tetrahedron; the maximum value 0.25 is reached for a regular tetrahedron. Moreover, the value 0.25 of both the MAXS and the MINS does not necessarily mean that the tetrahedron is regular−it may be a sliver-type (see Figure 8 in [25]). Other irregular tetrahedron with the vertices at (−0.001,0,0), (0.001,0,0), (0,−0.001,100) and (0,0.001,100) is a wedge-type one (see Figure 8 in [25]).

The numerical approximation of a gradient of a given function depends strongly on the largest angle (planar angle for a triangle and spherical or dihedral angle for a tetrahedron) [27]. Thus, the condition number of the stiffness matrix should be kept to a minimum.

Theoretically, to solve a partial differential equation numerically, the above mentioned quality measures Q_1–Q_5 should be as close to the ideal ones as possible for each of the mesh elements. However, not all deviations from the ideal have strong negative influence on the calculations with FEM. Moreover, it turns out that tetrahedrons with faces far from optimal are still of a quality enough to be used for numerical analysis of the model [23].

3.2. Mesh Boundary

If the structure to model is complex in a sense that it contains many substructures with their own surfaces which consist of triangles of very different size and quality then the generated mesh must take into account these substructures and the joints between them, which constitutes additional problems during the mesh generation.

The 3D mesh should be of a good quality not only in its 3D aspect but also in its 2D aspect as well. This concerns the quality of the surface of the mesh and, especially, the parts belonging to distinct areas.

The quality of a 2D (triangular) mesh of the surface of the bouton which topologically remains similar to the 3D ball is assessed analogically to the quality of the 3D net.

The quality measures that correspond to the ones defined for the spatial meshes are as follows: the square perimeter divided by the square root of the surface (PS2), the longest edge divided by the radius of the inscribed sphere (in that case the 2D sphere is a circle) (ER2), the longest edge divided by the smallest height (EH2) or the function of the ratio of the largest and smallest edge length, respectively, to the total perimeter of the triangle (MAXE and MINE).

Similar as in the 3D case, the best (the smallest) attainable values of the above measures (except MINE) are:

$PS2_{min} = 2x27^{1/4} \approx 4.55901$

$ER2_{min} = 2x3^{1/2} \approx 3.4641$

$EH2_{min} = 2/[3^{1/2}] \approx 1.1547$

$MAXE_{min} = 1/3 \approx 0.3333$

and the largest MINE is

$MINE_{max} = 1/3 \approx 0.3333$

For the first three measures the upper bound is infinity whereas for the fourth one (MAXE) it is equal to 0.5, and the lower bound for the last parameter (MINE) is 0.

3.3. Mesh Inconsistency

One of the possible faults of the mesh results from the fact that its boundary is not a closed surface and the meshing program is trying to create elements (tetrahedra) outside the bouton (*leaking*) which may happen when the intended common vertices of the adjacent tetrahedra separate, creating the gap between the walls. Another example of "leaking", termed as *double edge*, means that a cleft is created between the edges and the size of the cleft is less than one thousandth of the edge length. *Intersection* appears when the edge of one tetrahedron is intersecting with the face of another one; Some subset of the 3D mesh volume is then defined twice.

3.4. Mesh Quality

The measures of the mesh quality can by either the extreme values of the quality parameters or other parameters of the distribution of a parameter e.g., the maximum value of SV, ER, EH, or MINS, or minimum value of MAXS. These quantities, that are sometimes used to describe the mesh, and also the distributions themselves, are presented as tables and histograms.

4. Geometrical Models of the Bouton

The geometry of the bouton was modeled in three various ways, using three different objects.

Two of them−the geosphere and the ball (globe)−were extremely simplified models. The basic difference between geosphere surface mesh and globe surface mesh is that the geosphere surface consists only of triangles, nearly equally-shaped and nearly equilateral, whereas the globe surface contains two types of polygons: (1) equal isosceles (but not necessarily equilateral) triangles; and (2) trapezoids. The two above models are known to differ in some aspects. Two of them are most commonly mentioned. The first one is that with the globe mesh it is easier to create shapes with edges along meridians and circles of

latitude. The second one is that with the geosphere mesh it is easier to make a relatively smooth surface with a smaller number of mesh elements.

The third model, so-called real model, reflected the real geometry of the bouton surface and accounted for the presence of the inner organelles—see [20] for details.

4.1. Geosphere—The Simplest Model of the Sphere

The two-dimensional geosphere surface mesh, often used, for example in [18], to depict the surface of a sphere, consists of triangles, which are almost equilateral. Their characteristics exceed the ideal values by 1.3% to 25.5% which constitutes a good reference point for comparison of the quality of 3D meshes. The analyzed surface (Figure 1, left) had 15,680 triangular faces and 7482 vertices.
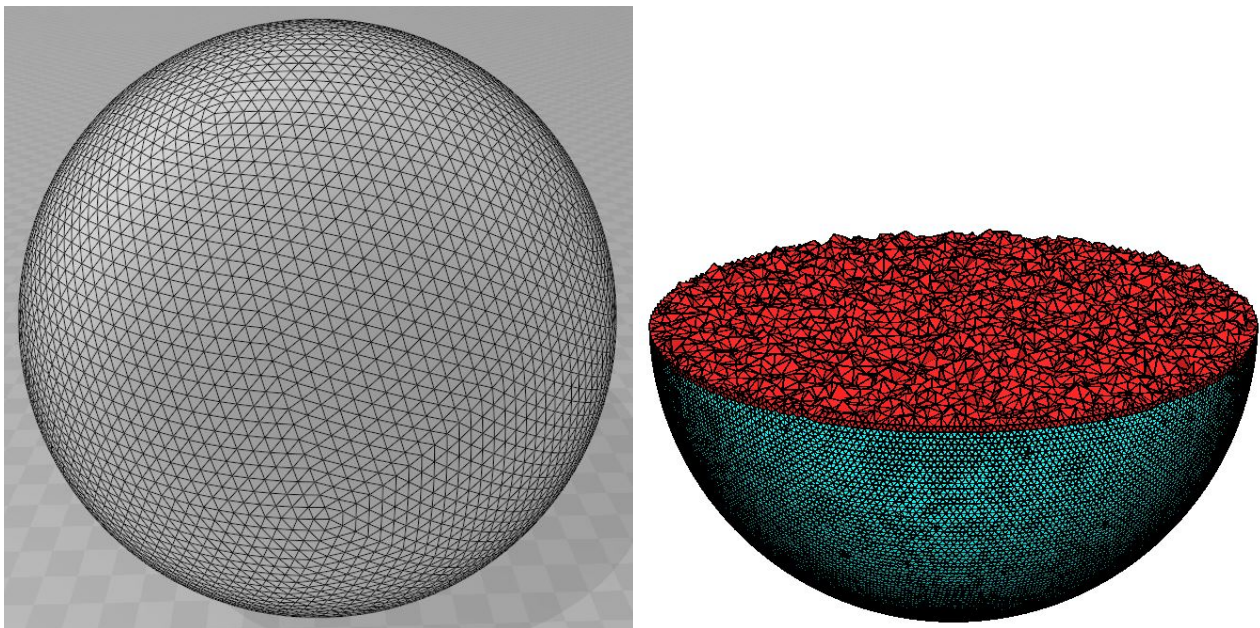
Figure 1. The surface (**left**) and the tetrahedral mesh (**right**) of a geosphere.

The quality of the model of the geosphere surface is presented in Table 1.

Table 1. Geosphere model surface mesh quality.

Name	Definition	Ideal	Min	Max	Max/Ideal
$PS2$	$P/\sqrt{S}$	$2\sqrt[4]{27} \approx 4.55901$	4.55903	4.6104	1.011
$ER2$	E_{max}/R	$2\sqrt{3} \approx 3.4641$	3.4684	3.9245	1.133
$EH2$	E_{max}/H_{min}	$2/\sqrt{3} \approx 1.1547$	1.1575	1.4527	1.258
$MAXE$	E_{max}/P	$1/3 \approx 0.3333$	0.3337	0.3702	1.111
$MINE$	E_{min}/P	$1/3 \approx 0.3333$	0.2913	0.3325	1.144 [1]

[1] This value is calculated differently—as ideal/min.

The angles of the triangular mesh considered in Table 1 vary between the values of 48.53° and 71.98°. The range of triangle area was from $S_{min} = 0.001903$ μm^2 to $S_{max} = 0.002051$ μm^2. Therefore, the ratio S_{max}/S_{min} was 107.8%. The surface mesh was then submitted as the input data to the TetGen program which produced the tetrahedral mesh of the sphere (Figure 1, right).

The parameters of the sphere were as in Table 2.

**Table 2.** Mesh quality of the geosphere 3D model.

Name	Definition	Ideal	Min	Max	Max/Ideal
SV	$\sqrt{S}/\sqrt[3]{V}$	$\sqrt[4]{3}\sqrt[6]{72} \approx 2.6843$	2.6844	4.7147	1.756
ER	E_{max}/R	$2\sqrt{6} \approx 4.8989$	4.9301	37.4427	7.643
EH	E_{max}/H_{min}	$\sqrt{3}/\sqrt{2} \approx 1.2247$	1.2398	14.628	11.944
$MAXS$	S_{max}/S	$1/4 = 0.2500$	0.2503	0.4434	1.774
$MINS$	S_{min}/S	$1/4 = 0.2500$	0.0639	0.2498	3.912 [1]

[1] This value is calculated differently−as ideal/min.

These parameters are the reference point for the next calculations.

4.2. The Ball (Globe)−The Simplest Geometric Model of the Presynaptic Bouton

The globe is a sphere divided into spherical polygons by meridians and circles of latitude. A typical globe is a depiction of the Earth's surface. For example, one may draw a globe with 24 meridians and 13 circles of altitude−or rather 11, if we exclude poles as degenerate circles. The simplest object used for modeling a presynaptic bouton [19] consisted of two such globes placed concentrically (see Figure 2).
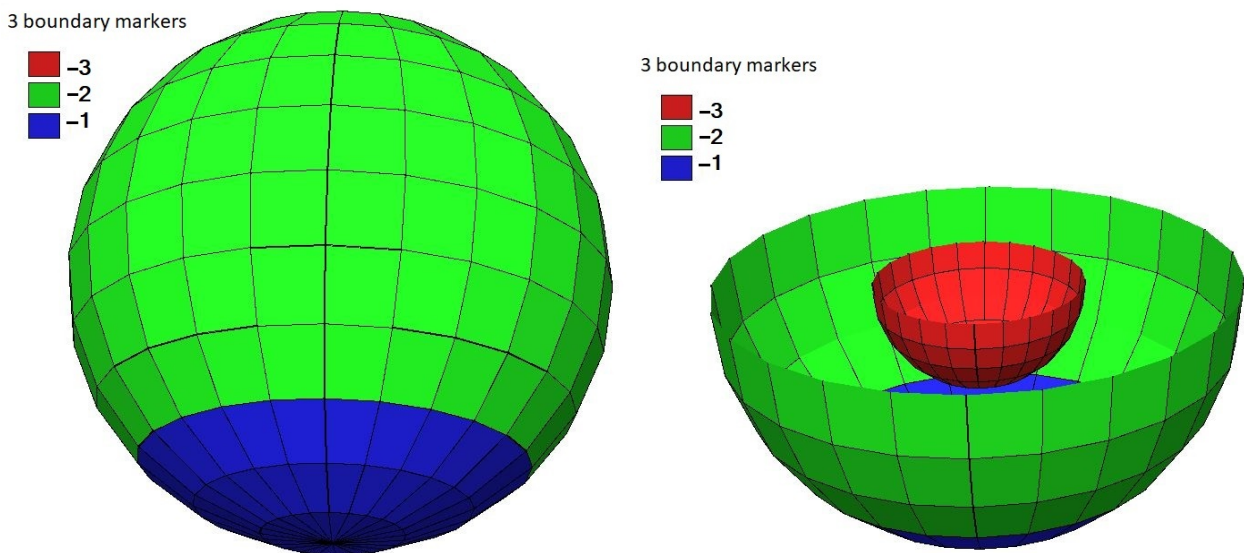
Figure 2. Wireframe structure of the surface of a 3D globe mesh. Bouton membrane—**green**, neurotransmitter release area—**blue**, supply zone boundary—**red**.

The input parameters for the meshing software were as follows: maximum volume of a single mesh element (tetrahedron) (VT_{max}). Another two important parameters are the maximum aspect ratio (EH_{max}) which is not standardized but computed directly as the ratio of the longest edge and the shortest height of a tetrahedron. The last restriction is that of the minimum dihedral angle (DA_{min}). It should be stressed that the last restriction is the most strictly observed in the program.

The 2-dimensional mesh is generated in such a way that each spherical polygon is replaced by a flat polygon with vertices at the same points. The quality of the globe mesh was tested in the following subspace of the above parameters:
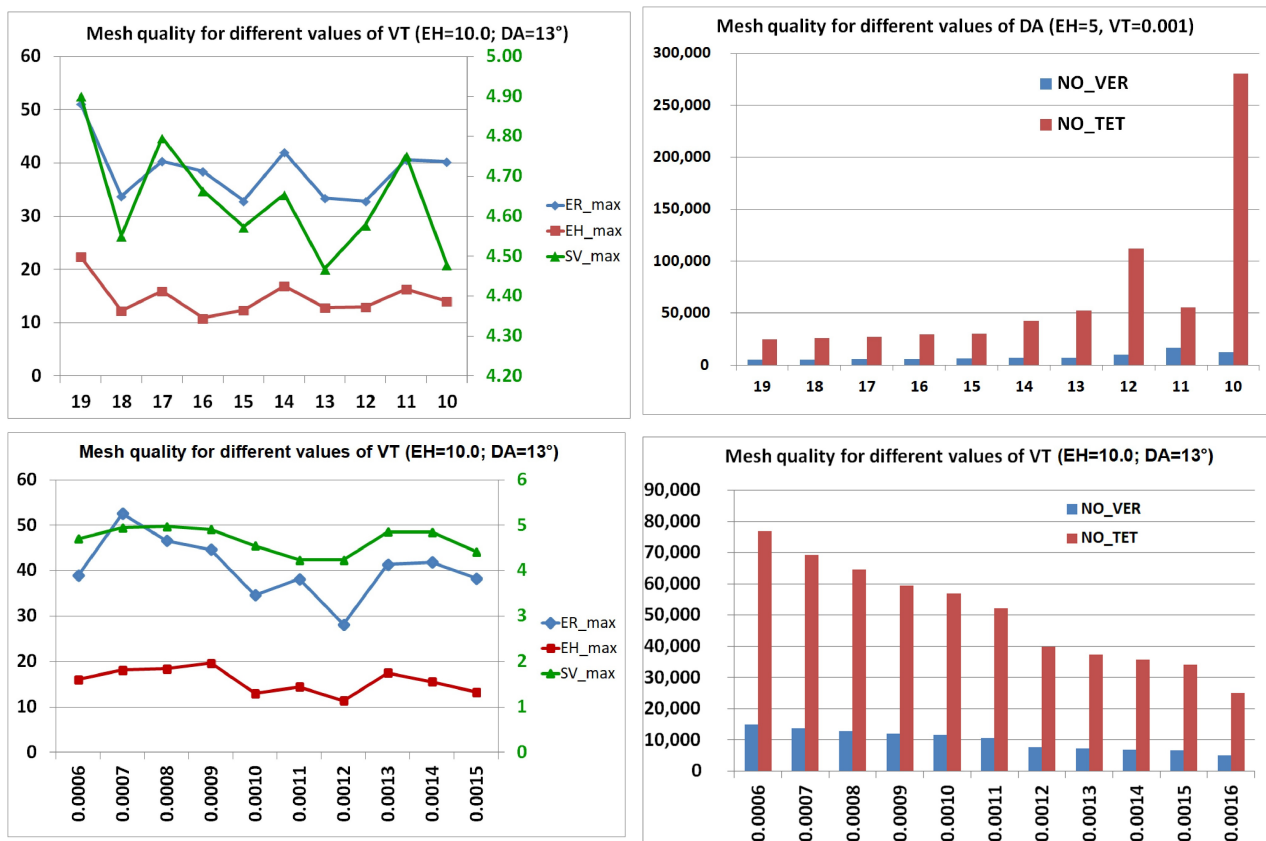
$$EH_{max} \in [4.0; 10.0]$$

$$VT_{max} \in [0.0006; 4.0]$$

$$DA_{min} \in [10°; 19°]$$

The example results of these tests are presented in Figure 3:

1. for the fixed values of $EH_{max} = 5$ and $VT_{max} = 0.001$ and for DA_{min} ranging from $10°$ to $19°$;
2. for the fixed values of $EH_{max} = 5$ and $DA_{min} = 13°$ and for VT_{max} ranging from 0.0006 to 0.0015.

The best quality was achieved when the imposed restrictions were: $EH_{max} = 10.0$, $DA_{min} = 13°$ and $VT_{max} = 0.0012$.

Figure 3. Quality of the 3D globe mesh assessed with the following measures: Left$-ER_{max}$, EH_{max} and SV_{max}. m right$-$number of vertices NO_VER and number of tetrahedra NO_TET. The mesh has been generated with TetGen program with the following parameters: minimum dihedral angle DA, maximum EH value, maximum element volume VT. The ranges of the axes are are **top**—fixed values of DA_{min} and VT_{max}, **bottom**—fixed values of EH_{max} and DA_{max}.

The input 2D mesh and the results of its tetrahedralization are presented in Tables 3 and 4.

Table 3. Mesh quality of the globe surface model.

Name	Definition	Ideal	Min	Max	Max/Ideal
$PS2$	$P/\sqrt{S}$	$2\sqrt[4]{27} \approx 4.55901$	4.55910	6.3549	1.394
$ER2$	E_{max}/R	$2\sqrt{3} \approx 3.4641$	3.4792	9.6114	2.775
$EH2$	E_{max}/H_{min}	$2/\sqrt{3} \approx 1.1547$	1.1647	4.5749	3.962
$MAXE$	E_{max}/P	$1/3 \approx 0.3333$	0.3348	0.4575	1.429
$MINE$	E_{min}/P	$1/3 \approx 0.3333$	0.1617	0.3325	2.061 [1]

[1] This value is calculated differently$-$as ideal/min.

Table 4. Mesh quality of the globe 3D model.

| Name	Definition	Ideal	Min	Max	Max/Ideal
SV	$\sqrt{S}/\sqrt[3]{V}$	$\sqrt[4]{3}\sqrt[6]{72} \approx 2.68433$	2.68503	4.23589	1.578
ER	E_{max}/R	$2\sqrt{6} \approx 4.89898$	4.97976	28.12424	5.741
EH	E_{max}/H_{min}	$\sqrt{3}/\sqrt{2} \approx 1.22474$	1.26564	11.40720	9.314
$MAXS$	S_{max}/S	$1/4 = 0.25$	0.25037	0.44492	1.780
$MINS$	S_{min}/S	$1/4 = 0.25$	0.06135	0.24977	4.075 [1]

[1] This value is calculated differently—as ideal/min.

4.3. The Real Model with Inner Organelles

In the real model, the shape of the bouton surface is created on the basis of the microscope image [28]−see [20] for details concerning the way the model is generated. Furthermore, the inner organelles−mitochondrion and microtubules−are also modeled as the inner structures of the bouton−Figure 4. In the model the following areas have to be taken into consideration: the area of the synapse membrane in general, the zone of releasing the neurotransmitter particles, the surface of the mitochondrion which in our model is connected to the artificially (i.e., numerically) cut bouton, the surface of the microtubules and of microtubule terminals. The above surfaces are marked with different colors in the graphs−Figure 5.
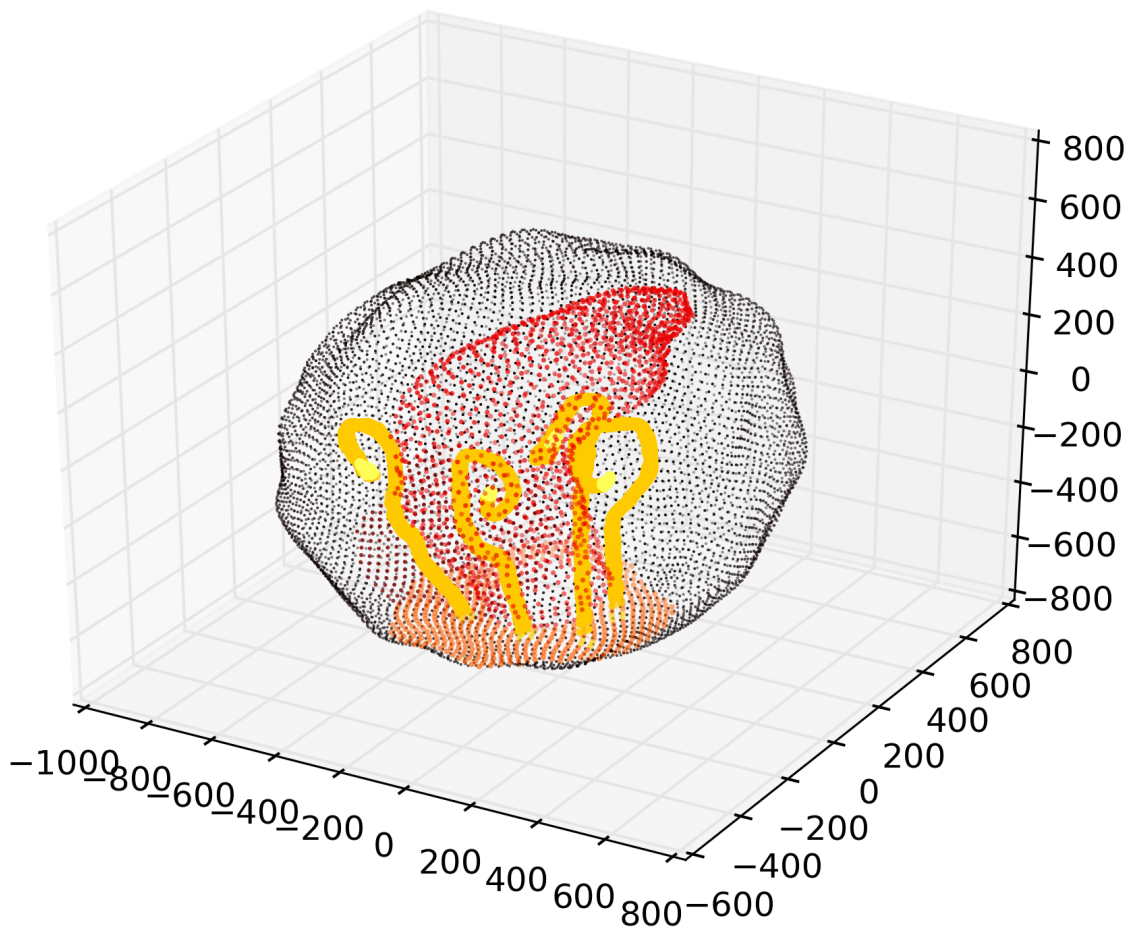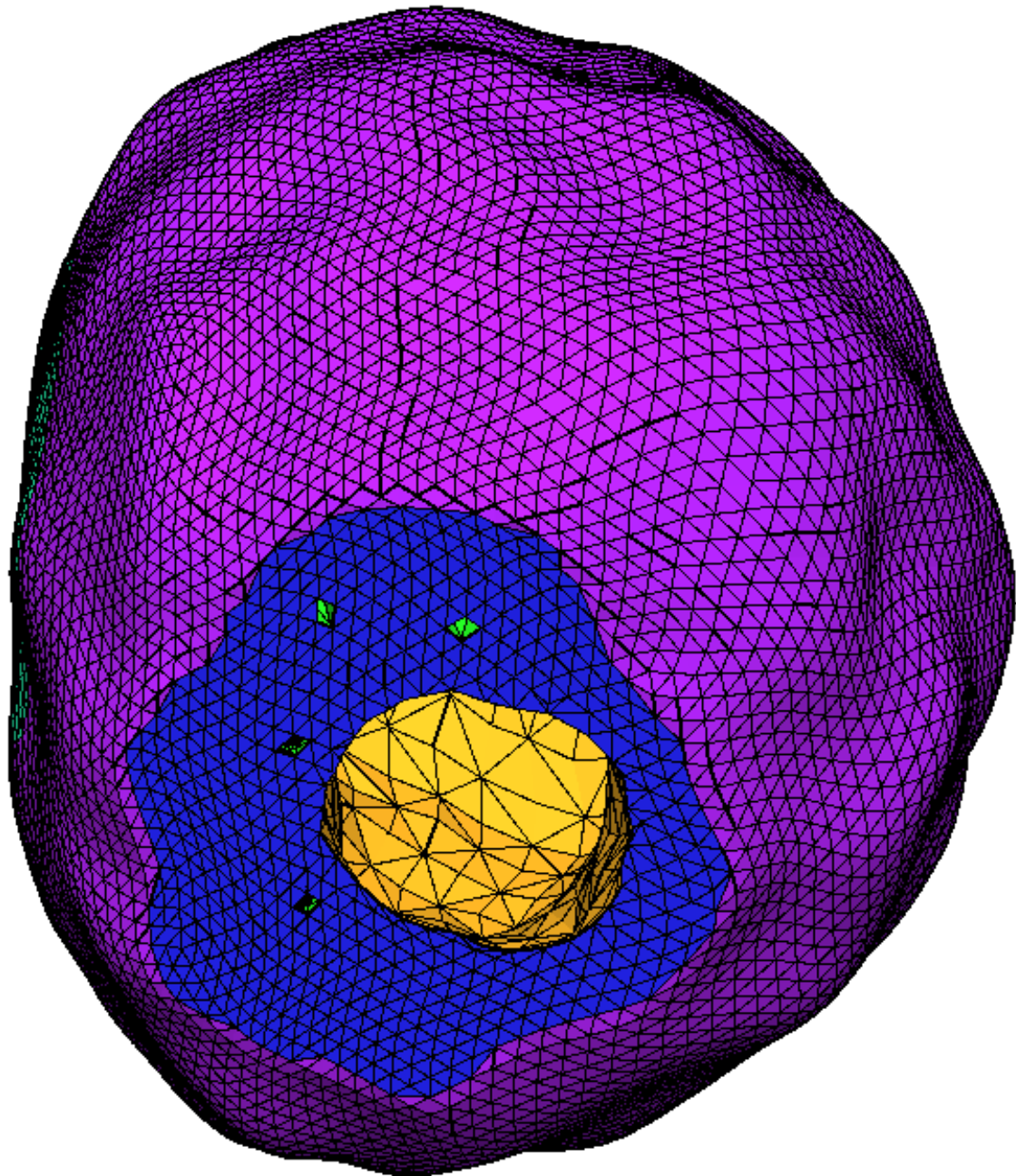

Figure 4. Real geometric model of the bouton with inner organelles—cell membrane (**black**), artificial cut (**orange**), mitochondrion (**red**) and microtubules (**yellow**) with their endings (**bright yellow**). The tick marks of the axes are placed at intervals of 200 nanometers.
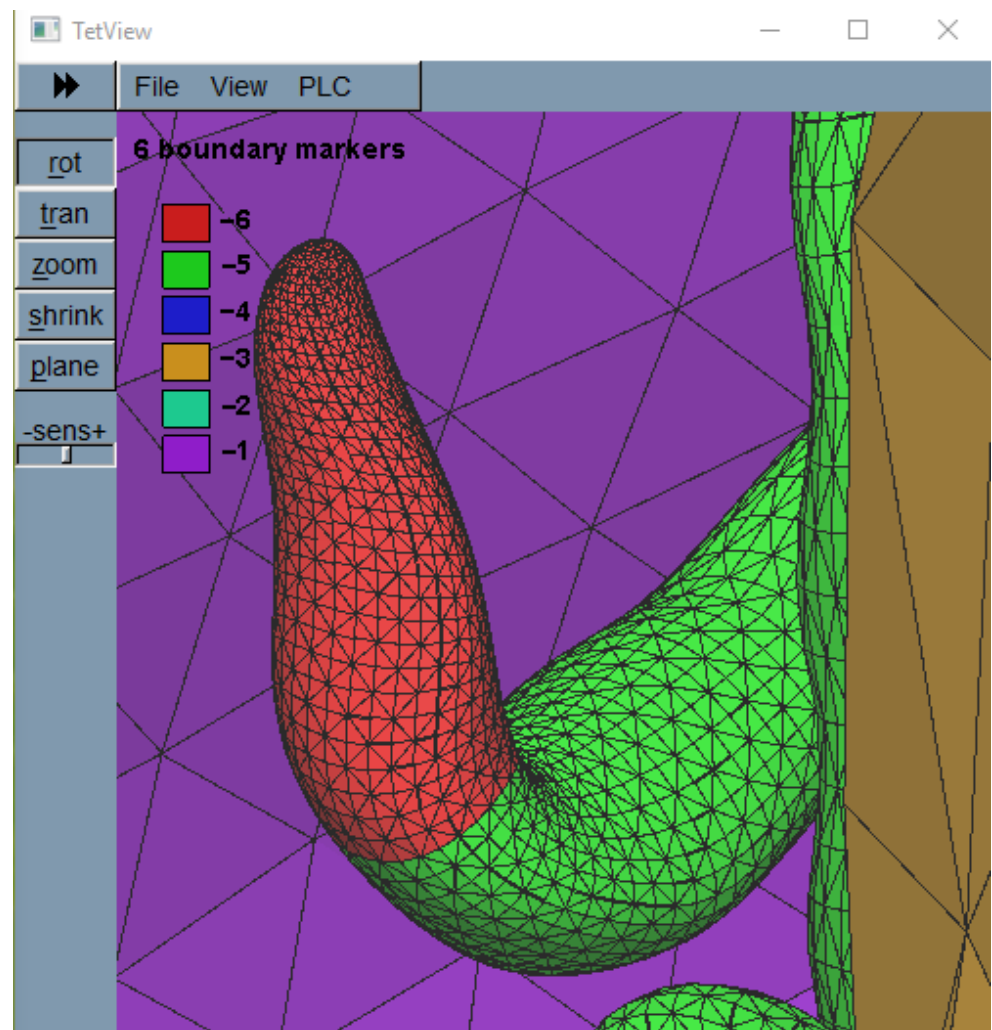
Figure 5. Microtubule with fitted surface mesh. The microtubule terminal−**red** (−6), the body of the microtubule−**green** (−5), mitochondrion−**gold** (−3), membrane−**purple** (−1).

The input mesh was made up of 41,807 vertices and 83610 triangles—Figure 6. Generation of the three-dimensional mesh in such a way that the triangular faces of the mesh tetrahedra constitute the two-dimensional mesh covering the surfaces of the inner structures, especially when small details are concerned, was one of the crucial problems (Figures 5–9, in particular Figure 5 and Figure 9, see also [17]). The characteristics of the input mesh are presented in Table 5.

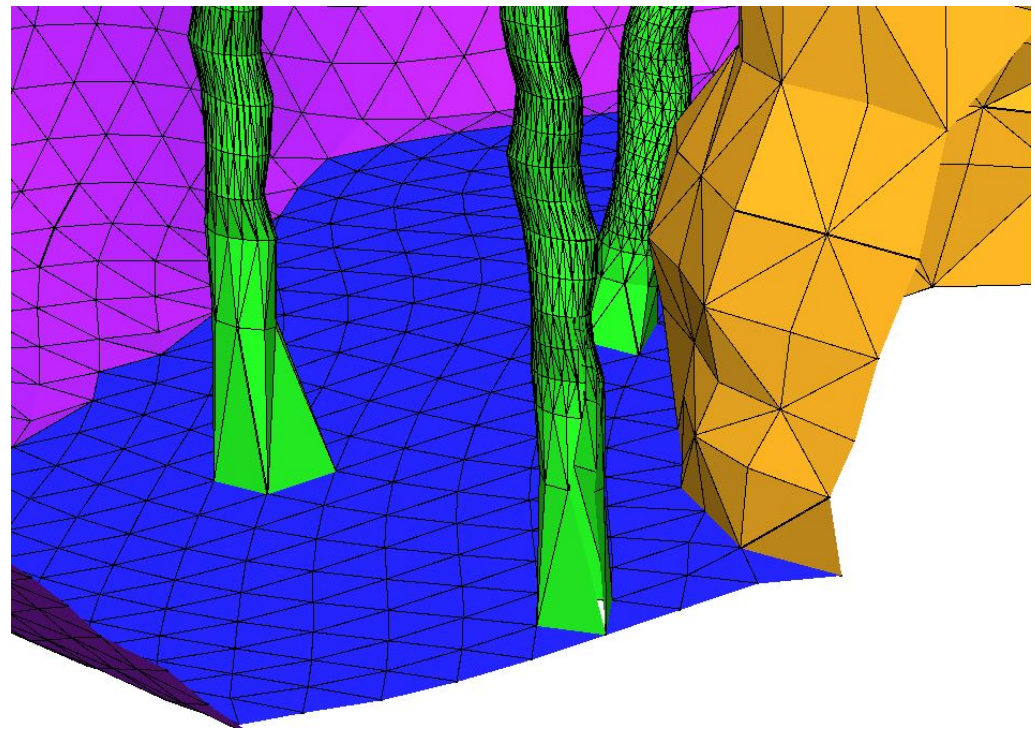**Figure 6.** The two dimensional surface mesh of the real geometric model of the bouton. Microtubule—**green**, artificial cut—**blue**, mitochondrion—**gold**, membrane—**purple**.
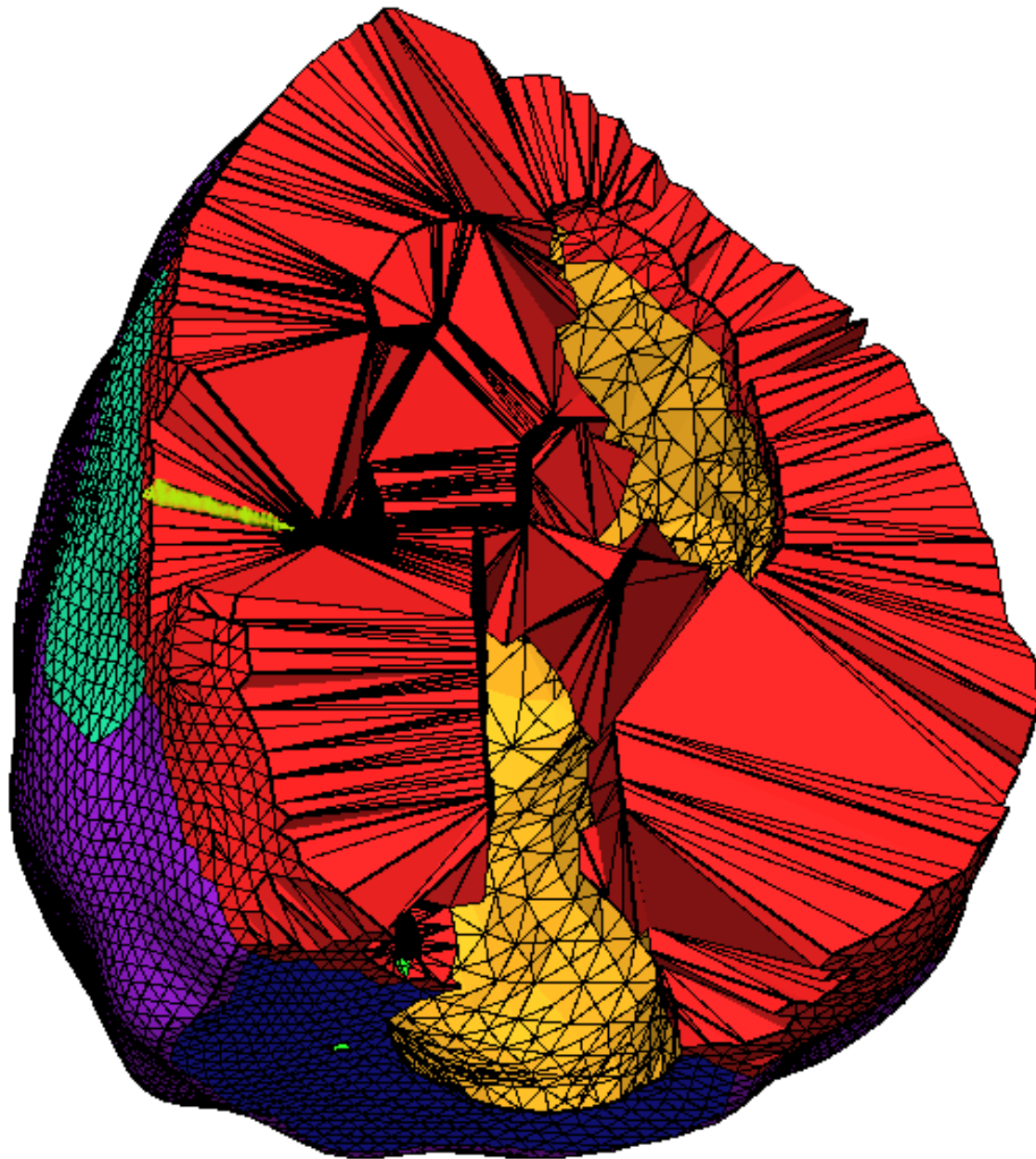
Figure 7. The real geometric model of the bouton filled by a three-dimensional mesh fitted to the two dimensional mesh shown in Figure 6. The mesh has been generated by using TetGen with no optimization. The quality of the mesh is very low because of the presence of a lot of needle-shaped tetrahedra what can be observed in the cross section. The artificial cut—**blue**, the inside of the mitochondrion—**yellow**, the surface of the bouton—**purple**, the cut surface—**red**. An example tetrahedron that has one vertex in the synthesis zone and the other in the release site is marked with bright lime color.
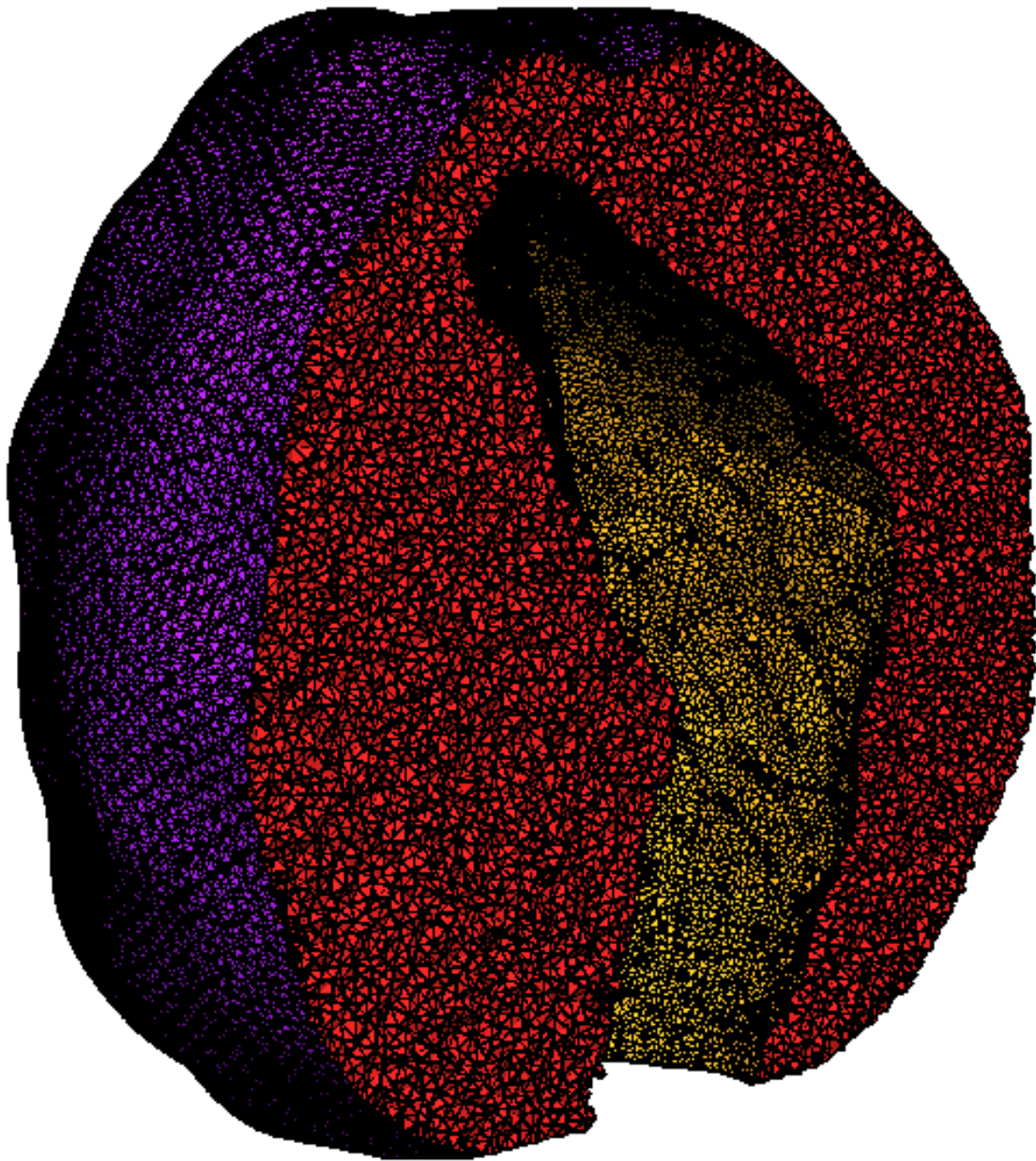
Figure 8. The real geometric model of the bouton filled by a three-dimensional mesh fitted to the two dimensional mesh shown in Figure 6. The mesh has been generated by using TetGen and it has been optimized by applying the operations such as: node smoothing, edge/face swapping, edge contraction, and vertex insertion. The artificial cut—**blue**, the inside of the mitochondrion—**yellow**, the surface of the bouton—**purple**. On the right—the section. The cut plane—**red**, the inner of the mitochondrion—**yellow**.

Figure 9. The membrane of the bouton (**purple**), the artificial cut surface (**blue**), fragments of the microtubules (**green**) and a fragment of the mitochondrion (**yellow**) with surfaces covered by triangles−two-dimensional mesh.

Table 5. Surface mesh quality of the real 3D model.

Name	Definition	Ideal	Min	Max	Max/Ideal
$PS2$	$P/\sqrt{S}$	$2\sqrt[4]{27} \approx 4.55901$	4.55902	21.12052	4.633
$ER2$	E_{max}/R	$2\sqrt{3} \approx 3.4641$	3.4684	111.47228	32.179
$EH2$	E_{max}/H_{min}	$2/\sqrt{3} \approx 1.1547$	1.15740	55.71270	48.249
$MAXE$	E_{max}/P	$1/3 \approx 0.33333$	0.33372	0.49979	1.499
$MINE$	E_{min}/P	$1/3 \approx 0.3333$	0.04002	0.33296	8.329 [1]

[1] This value is calculated differently—as ideal/min.

The above input mesh was passed as input data to the TetGen program. The program generated output mesh with no optimization, thereby the result was deliberately of a very poor quality. The parameters of the output tetrahedral mesh are presented in Table 6. The mesh had 57,060 nodes, 114,116 boundary faces and 194,064 tetrahedra.

Table 6. Mesh quality of the real 3D model−the worst mesh.

Name	Definition	Ideal	Min	Max	Max/Ideal
SV	$\sqrt{S}/\sqrt[3]{V}$	$\sqrt[4]{3}\sqrt[6]{72} \approx 2.684$	2.703	52.387	19.516
ER	E_{max}/R	$2\sqrt{6} \approx 4.8990$	5.7381	52,443.6	107,049.6
EH	E_{max}/H_{min}	$\sqrt{3}/\sqrt{2} \approx 1.2247$	1.5641	262,212.2	214,095.4
$MAXS$	S_{max}/S	$1/4 = 0.25000$	0.25002	0.499995	1.99998
$MINS$	S_{min}/S	$1/4 = 0.25000$	0.000009	0.24998	28,444.1 [1]

[1] This value is calculated differently—as ideal/min.

The next step was, as it has been done previously, to generate the optimized mesh. Its quality was checked for different values of input TetGen parameters. Those parameters after preliminary tests were set to

$EH_{max} \in [70; 100]$

$DA_{min} \in [1°; 20°]$

$VT_{max} = 1000 \ \mu m^3$

The best quality was achieved for $EH_{max} = 100; DA_{min} = 2°; VT_{max} = 1000$.

The size of the mesh was 391,897 nodes, 4,141,116 faces (296,528 on the bouton surface) and 1,996,426 tetrahedra.

The distributions of the values of the parameters are given in Figures 10–12 and in Table 7.

Table 7. Mesh quality of the real 3D model after optimization with TetGen program.

Name	Definition	Ideal	Min	Max	Max/Ideal
SV	$\sqrt{S}/\sqrt[3]{V}$	$\sqrt[4]{3}\sqrt[6]{72} \approx 2.68433$	2.68435	8.83147	3.290
ER	E_{max}/R	$2\sqrt{6} \approx 4.8990$	4.9108	605.693	123.636
EH	E_{max}/H_{min}	$\sqrt{3}/\sqrt{2} \approx 1.2247$	1.2308	301.5059	246.127
$MAXS$	S_{max}/S	$1/4 = 0.25000$	0.25001	0.49804	1.992
$MINS$	S_{min}/S	$1/4 = 0.25000$	0.00228	0.24999	109.649 [1]

[1] This value is calculated differently—as ideal/min.
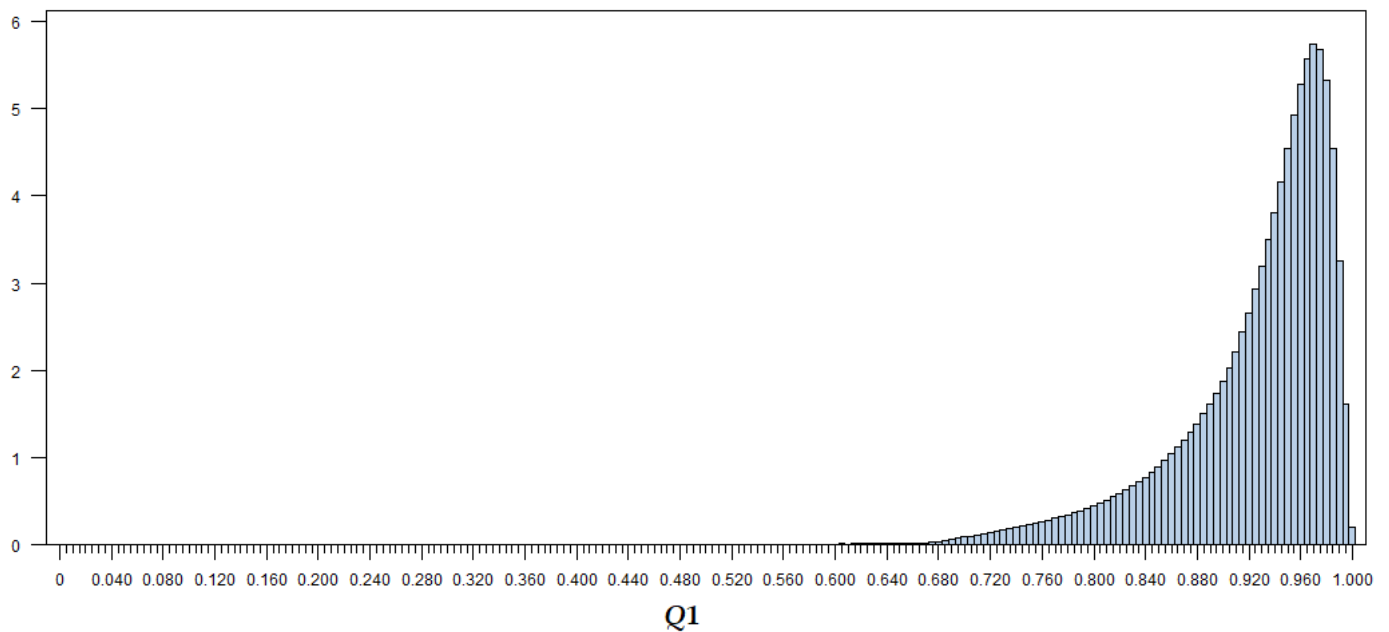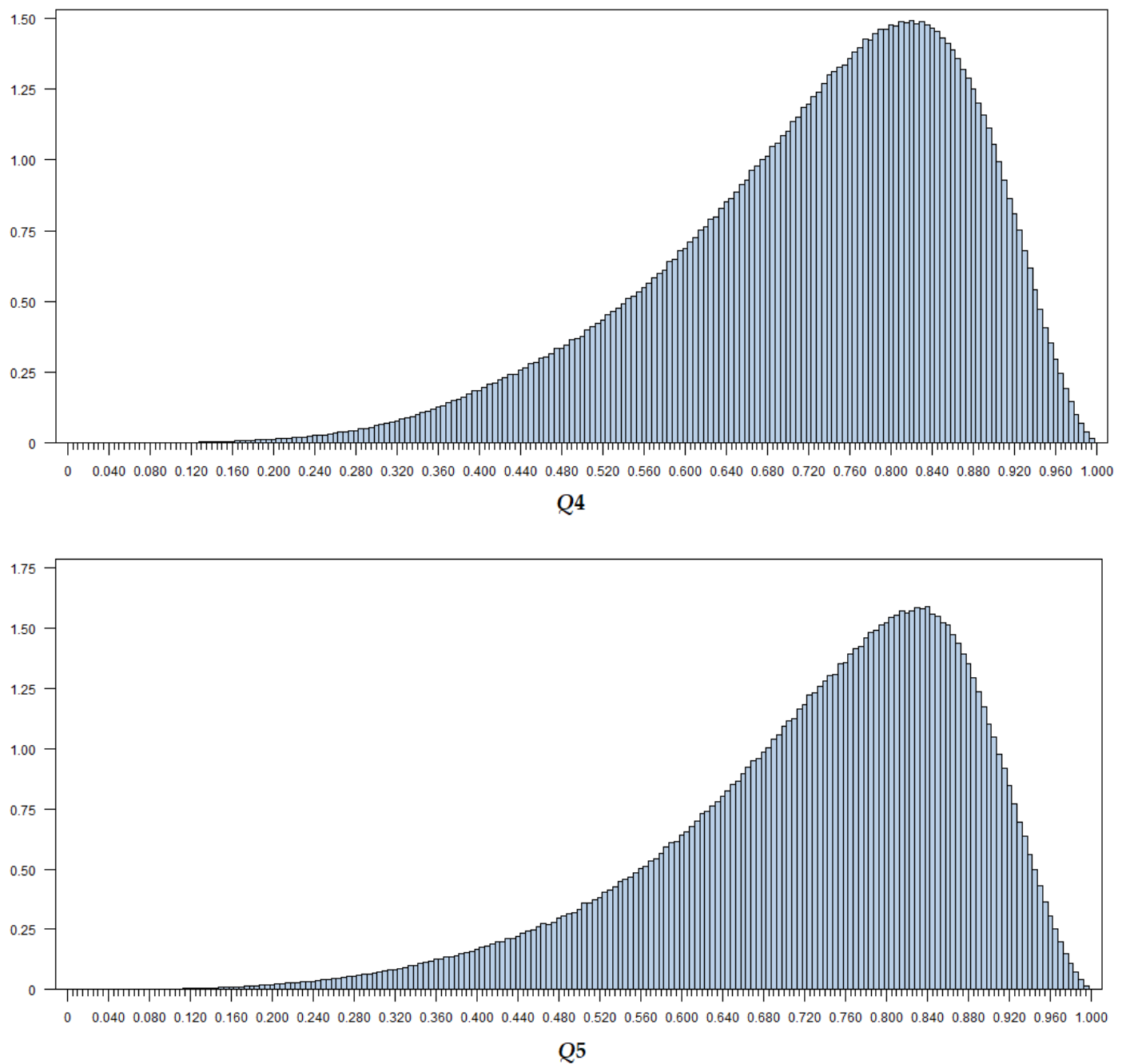

Figure 10. Distribution of the quality measure Q_1 (standardized version of SV), of the mesh of the real model of the bouton. Probability (percent)—vertical axis.
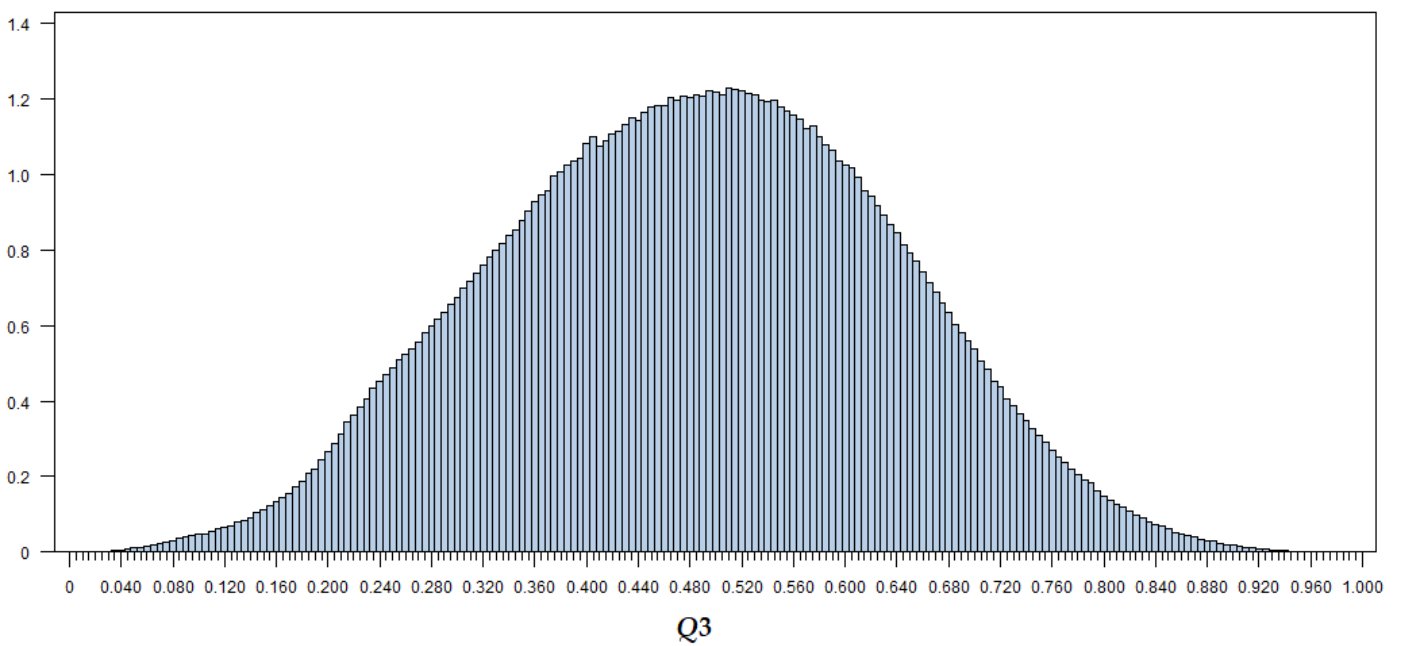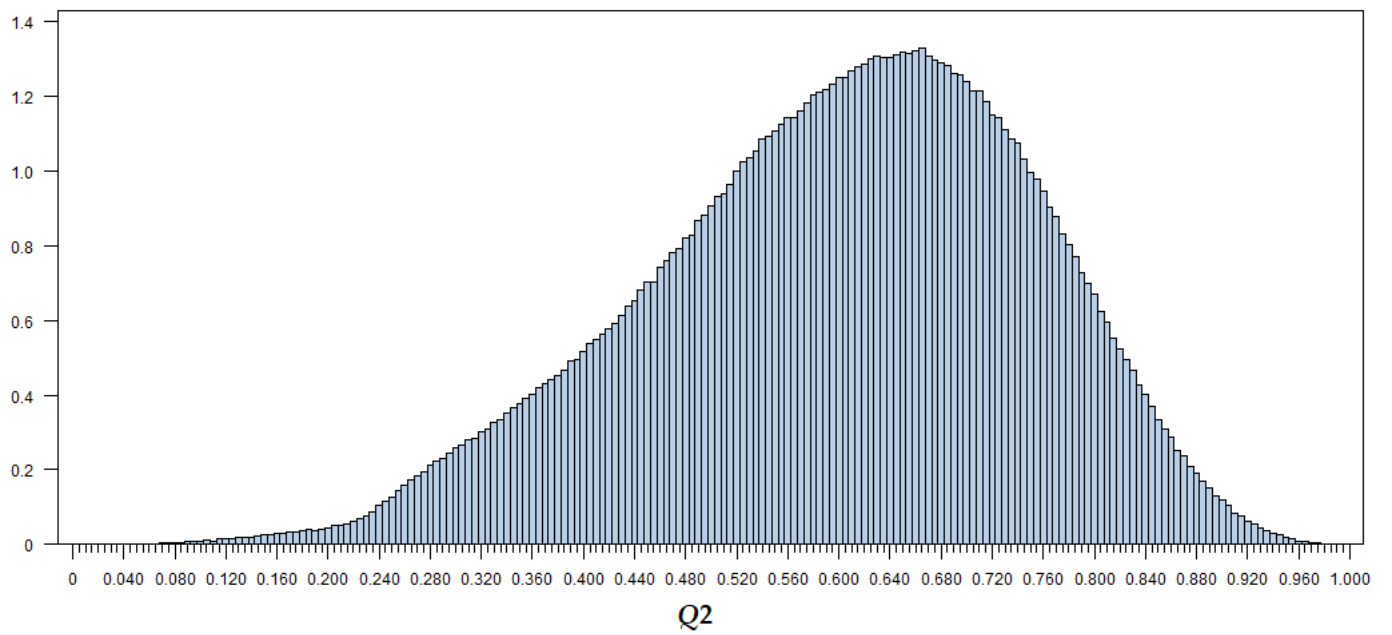
Figure 11. Distributions of the quality measures Q_2 (standardized version of EH) and Q_3 (standardized version of ER), of the mesh of the real model of the bouton. Probability (percent)—vertical axis.

Figure 12. Distributions of the quality measures Q_4 (standardized version of MX) and Q_5 (standardized version of MN), of the mesh of the real model of the bouton. Probability (percent)—vertical axis.

5. First Comparison of the Models

The quality of all 3D meshes of the models are given in Table 8. The smallest values are always close to the ideal ones; the relative differences was always below 1.23% so those minimal numbers are not presented.

For the simplified models of the bouton (the geosphere and the globe) Table 8 the distance between the mean and the median lay within the range of two standard deviations of the corresponding parameter.

Table 8. Mesh quality measures of all the models.

Name	Definition	Ideal	Mean	SD	Median	P90	P99	Max
		GEOSPHERE:						
SV	$\sqrt{S}/\sqrt[3]{V}$	$\sqrt[4]{3}\sqrt[6]{72} \approx 2.68433$	2.84749	0.15648	2.79918	3.03451	3.46124	4.71468
ER	E_{max}/R	$2\sqrt{6} \approx 4.89898$	7.78874	1.82397	7.38168	9.92162	14.42310	37.44269
EH	E_{max}/H_{min}	$\sqrt{3}/\sqrt{2} \approx 1.22474$	2.38374	0.66151	2.24651	3.20865	4.62071	14.62800
$MAXS$	S_{max}/S	$1/4 = 0.25$	0.30413	0.02705	0.30016	0.34145	0.37957	0.44339
$MINS$	S_{min}/S	$1/4 = 0.25$	0.19808	0.02518	0.20173	0.16303 [1]	0.15112 [1]	0.06385 [1]
		GLOBE:						
SV	$\sqrt{S}/\sqrt[3]{V}$	$\sqrt[4]{3}\sqrt[6]{72} \approx 2.68433$	2.88477	0.20380	2.81796	3.11881	3.74693	4.23589
ER	E_{max}/R	$2\sqrt{6} \approx 4.89898$	8.20721	2.40916	7.56507	10.90243	18.32399	28.12424
EH	E_{max}/H_{min}	$\sqrt{3}/\sqrt{2} \approx 1.22474$	2.54553	0.85918	2.32799	3.59229	5.75653	11.40720
$MAXS$	S_{max}/S	$1/4 = 0.25$	0.30769	0.02907	0.30364	0.34783	0.38617	0.44492
$MINS$	S_{min}/S	$1/4 = 0.25$	0.19443	0.02878	0.19953	0.15380 [1]	0.13958 [1]	0.06135 [1]
		REAL MODEL:						
SV	$\sqrt{S}/\sqrt[3]{V}$	$\sqrt[4]{3}\sqrt[6]{72} \approx 2.68433$	2.950	0.329	2.821	3.347	4.284	8.831
ER	E_{max}/R	$2\sqrt{6} \approx 4.89898$	9.690	6.777	7.535	15.175	37.042	605.693
EH	E_{max}/H_{min}	$\sqrt{3}/\sqrt{2} \approx 1.22474$	3.177	3.046	2.259	5.347	15.732	301.506
$MAXS$	S_{max}/S	$1/4 = 0.250$	0.310	0.042	0.299	0.373	0.445	0.498
$MINS$	S_{min}/S	$1/4 = 0.250$	0.188	0.048	0.205	0.110 [1]	0.077 [1]	0.002 [1]

[1] In this row the values P90, P99 and max are replaced with P10, P5 and min, respectively.

For the real model of the bouton, that takes into consideration the same parameters, the situation was noticeably worse, although it still remained satisfactory. The specified 90th and 99th percentiles were similar for all three models. The maximal values in the case of the real bouton mesh were, however, over one order of magnitude (approximately 30 times) larger than the corresponding values for the simpler models which means that there are some bad quality mesh elements. Nevertheless, their number is extremely low in comparison to the total number of the mesh tetrahedra.

If the simplest structures are to be taken as the reference points for assessing the quality of the real mesh, it must be admitted that the extreme values of the quality parameters (non-standardized) were significantly higher than those reference values. The percentage of the "bad" tetrahedra was, however, low−below 1%, which means that, in general, the meshes were suitable as the input for subsequent optimizations.

6. Further Optimizations Involving Modifications of the Surface and Improvement of Dihedral Angles

The results of examination of the created meshes, particularly the real one, revealed problems with their quality, mainly concerning the distribution of dihedral angles of mesh elements, so additional modifications were needed. That was accomplished by using the Stellar software [29]. Next, the simulation results for the worst mesh were compared with those for the best one.

The Stellar program performs transformations like inserting and deleting vertices, edge contraction, smoothing or removing boundary or near-boundary nodes, removal of boundary edges, multi-face removal and, in addition, compound operations which means combinations of all the above transformations.

Stellar software focuses mainly on correcting dihedral angles of mesh tetrahedra which, according to the author, is crucial for numeric calculations (see [29] and the relevant references therein). The results of improving that parameter are in Table 9 for the three models presented above.

Table 9. Mesh quality improvement with Stellar software for all the models (for the real model the worst, "raw", mesh is also included).

Improv. Stage	Number of Nodes	Number of Faces	Number of Tetrahedra	Ideal DA	Min DA	Max DA	Improv. (Min)	Improv. (Max)
			GEOSPHERE:					
before	121,358	63,196	644,999	70.53°	5.83°	164.92	−	−
after	125,915	64,062	472,414	70.53°	37.50	140.41	6.43	1.17
			GLOBE:					
before	7567	6354	39,853	70.53°	7.90°	162.18°	−	−
after	8850	5096	26,283	70.53°	37.44°	139.46°	4.74	1.16
			REAL MODEL:					
worst	57,060	114,116	194,064	70.53°	0.0038°	179.915°	−	−
before	391,897	296,528	1,996,426	70.53°	0.528°	175.383°	201.06	1.03
after	572,775	357,578	1,635,827	70.53°	19.727°	160.273°	37.33	1.09

The extreme values of the parameters SV, ER, EH, MAXS and MINS after improving the mesh are given in Table 10.

Table 10. Mesh quality measures of all the models after improvement.

Name	Definition	Ideal	Mean	SD	Median	P90	P99	Max
			GEOSPHERE:					
SV	$\sqrt{S}/\sqrt[3]{V}$	$\sqrt[4]{3}\sqrt[6]{72} \approx 2.68433$	2.80129	0.06310	2.79255	2.88640	2.97954	3.33775
ER	E_{max}/R	$2\sqrt{6} \approx 4.89898$	7.47835	1.29978	7.26340	9.07162	11.85719	24.99427
EH	E_{max}/H_{min}	$\sqrt{3}/\sqrt{2} \approx 1.22474$	2.31219	0.54216	2.21765	2.98423	4.11482	9.75960
$MAXS$	S_{max}/S	$1/4 = 0.25$	0.30716	0.02864	0.30297	0.34659	0.38850	0.43438
$MINS$	S_{min}/S	$1/4 = 0.25$	0.19643	0.02555	0.19967	0.16305 [1]	0.14975 [1]	0.04684 [1]
			GLOBE:					
SV	$\sqrt{S}/\sqrt[3]{V}$	$\sqrt[4]{3}\sqrt[6]{72} \approx 2.68433$	2.81312	0.06964	2.80272	2.90532	3.01900	3.21246
ER	E_{max}/R	$2\sqrt{6} \approx 4.89898$	7.76157	1.49536	7.47481	9.66496	12.82559	19.98282
EH	E_{max}/H_{min}	$\sqrt{3}/\sqrt{2} \approx 1.22474$	2.46626	0.66469	2.33056	3.31735	4.71825	7.41859
$MAXS$	S_{max}/S	$1/4 = 0.25$	0.31461	0.03285	0.30945	0.36080	0.40590	0.43614
$MINS$	S_{min}/S	$1/4 = 0.25$	0.18995	0.02885	0.19390	0.15030 [1]	0.13593 [1]	0.06181 [1]
			REAL MODEL:					
SV	$\sqrt{S}/\sqrt[3]{V}$	$\sqrt[4]{3}\sqrt[6]{72} \approx 2.68433$	2.87951	0.14403	2.84965	3.03650	3.37273	6.39540
ER	E_{max}/R	$2\sqrt{6} \approx 4.89898$	9.41086	6.40490	8.34152	12.62199	24.68540	838.46663
EH	E_{max}/H_{min}	$\sqrt{3}/\sqrt{2} \approx 1.22474$	3.17968	2.74576	2.71390	4.63019	9.51595	383.60024
$MAXS$	S_{max}/S	$1/4 = 0.250$	0.32890	0.03993	0.32307	0.38640	0.43094	0.48228
$MINS$	S_{min}/S	$1/4 = 0.250$	0.17597	0.03685	0.18143	0.12600 [1]	0.10764 [1]	0.00286 [1]

[1] In this row the values P90, P99 and max are replaced with P10, P5 and min, respectively.

7. Simulations

As it has been mentioned above, the last method applied in this paper to compare the quality of meshes was to run example simulations for the different meshes of the same object and comparing the results. The three 3d "real" meshes were chosen: the mesh with no improvement, the one improved by TetGen and the mesh which was additionally optimized with Stellar. The parameters for all three simulations were the same: the size and shape of the surface mesh, the initial density distribution of neurotransmitter (NT), the

time step assumed for the calculations and the time interval during which the release of NT took place.

The values determining the results used in this paper were: diffusion coefficient $a = 3.0 \ \mu m^2/s$, permeability coefficient $\alpha = 416 \ \mu m^3/s$, the time step $t = 0.0001$ s and the time interval during which the release occurred—from $t = t_0 + 0.0022$ s to $t = t_0 + 0.0027$ s.

The criterion used to compare the results was the amount of neurotransmitter released during the first release time interval i.e., from $t = 0.0022$ s to $t = 0.0027$ s, which embraced 6 consecutive time steps. The additional criterion connected with the first one was the total amount of NT in the bouton.

8. Results

The results are presented in Figure 13. Three plots break down naturally in two groups. The two lower ones, depicting the total amount of neurotransmitter (NT) in the bouton varying in time, are almost identical. The values for the mesh improved with Stellar are only a little lower. This may be attributed to the fact that the total amount of NT was calculated based from the values of the density function in mesh vertices which differed in number and location between meshes. The upper plot (black) refers to the initial unimproved mesh. Its values are remarkably higher and the differences are clearly visible; nearly doubled values at the beginning of the impulse and equal values at the end.
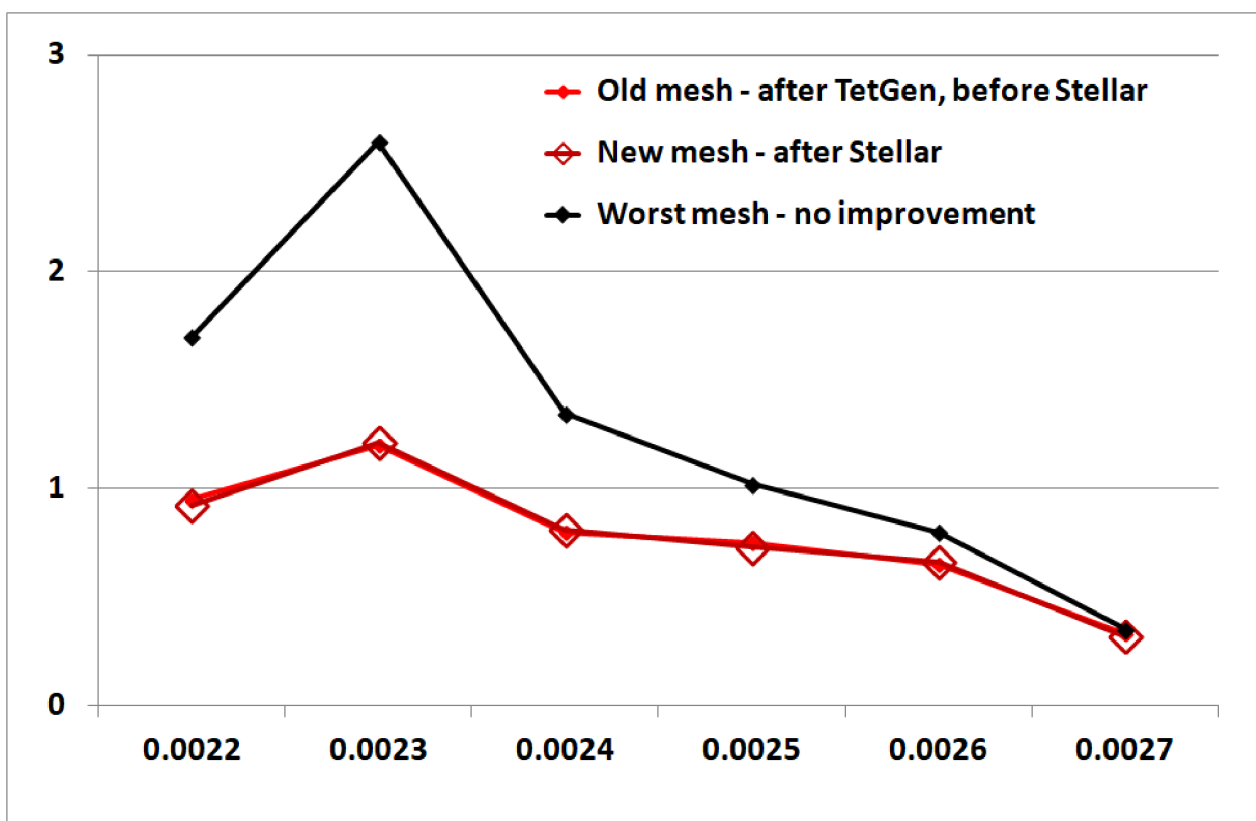
Figure 13. Comparison of simulation results for three various meshes. The plot represents the amount of neurotransmitter released during stimulation by a single incoming electrical impulse.

Two out of five values of the real mesh parameters presented in Table 8 increased remarkably after applying Stellar optimization. Namely, the maximal value of ER changed from 605.7 to 838.5 and the maximum of EH—from 301.5 to 383.6. The corresponding 95th percentiles decreased which means that only a very small fraction of the tetrahedra had worse ER or EH quality. The maximal (in case of MINS, minimal) values and the 95th (for MINS, the 5th) percentiles of of all other parameters improved after optimization. The interesting outcome of the optimization is that the only parameter that showed substantial

improvement was the one designed for this paper i.e., the SV parameter which changed from 8.83 to 6.40 (a nearly 30% better value). The results confirm that the parameter SV could be calculated instead of six dihedral angles of a tetrahedron. With the improved mesh, simulation of neurotransmitter flow in the examined model should be performed with sufficient precision. The detailed inspection of the accuracy of these calculations will be the subject of further research.

It should be stressed that the mesh analyzed in this paper is quite a complicated one which can be confirmed by the fact that the output mesh quality measured by dihedral angles was only in the range of 19 to 160 degrees. When we take into consideration the statement from [29]: *"My implementation usually improves meshes so that no dihedral angle is smaller than 34° or larger than 131°"*, it must be concluded that the mesh considered here is extremely complicated.

9. Effect of Mesh Quality on the Algorithm Performance and Results of Simulations

The algorithm, basically, consists of two modules. The first one is responsible for calculations initialization. Among others, it initializes the vector of the unknown variables i.e., the density vector ρ. The second one performs iterative calculations over time and space mesh.

In the second module, the iterative one, the calculations in each iteration are divided into three steps: the first one, during which the equation system is solved without taking release and synthesis into consideration, the second one when the values of the vector ρ are updated with the synthesis, and the third one, that involves the diminishing the value of the neurotransmitter density by the amount resulting from the exocytosis. Within the second said step, solving the equation system must be repeated until the status of each tetrahedron—"producing" or "non-producing"—is established between iterations. This means, among others, that calculations on a single tetrahedron may cause the program get stuck in the loop in case when the tetrahedron has one vertex in the release zone and another one in the synthesis zone. Such vertices exist in the worst, unimproved mesh in the real model.

In general, the comparison of calculations for different meshes is a difficult task. The reason is that vertices of different meshes covering the same object, are usually not identical. Therefore it is not possible to compare results obtained in the same mesh points. In the case of modeling the dynamics of transmitting signals in synapse, however, the situation is convenient because the total release of neurotransmitter into synaptic cleft in the time unit is a direct effect of the run of the processes occurring in the presynaptic bouton. This directness is guaranteed by the fact that the presynaptic bouton, considered as a cybernetic system, has the observability property [6].

Referring to the conducted simulations, the phenomena mentioned above are visible clearly. First of all, for the worst unimproved mesh, the calculations with the synthesis turned on got stuck in a loop because of existence of tetrahedra that intersect both the release area and the synthesis area. Such an example tetrahedron is marked bright lime in Figure 7.

In the case of simulation without synthesis, the total amount of neurotransmitter released into the synaptic cleft differs by a factor of around two, for the worst mesh (Mesh 1) compared to the middle-quality one (Mesh 2) and the best mesh (Mesh 3) which both give practically the same result—see Figure 13 and Table 11. The remarkable difference in the simulated amount of released neurotransmitter means, among others, that even in the case of a simple dynamic model—diffusive-reactive PDE model—the use of a mesh of a poor quality produces results which do not reflect the real solutions. It must be admitted that the shape of the impulse is maintained, and that can be confirmed by comparing impulses conducted via calcium channels measured by other authors [2,3] with the result of our research. In all the papers, including this one, the impulses were V-shaped. It should be also noted that the amount of the released NT, used in this paper, is a very accurate indirect measure of the postsynaptic potential (see Figure 1A in the related work [3]).

The peak of the impulse, however, is higher for the worst mesh (Figure 13) which would lead to false conclusions. In genetic research this could even favor the object which produces higher output amplitude as more heterozygous since homozygosity usually means impairing life processes (see a related paper [4], especially Figure 3C therein).

Table 11. Release of neurotransmitter during exocytosis phase for three different meshes of the real bouton model [vesicles/time step]. Mesh 1—the worst mesh, Mesh 2—Mesh 1 improved with TetGen, Mesh 3—Mesh 2 improved with Stellar

Time[s]	Mesh 1	Mesh 2	Mesh 3
0.0022	1.67572458	0.93988859	0.91254579
0.0023	2.52562556	1.25460856	1.25423054
0.0024	1.42968640	0.76737063	0.77887697
0.0025	1.01510141	0.71655252	0.71123427
0.0026	0.80204156	0.59739848	0.60125321
0.0027	0.36672566	0.33349662	0.32721117

The performed simulations, furthermore, shed−to some extent−light on the problem of the mesh quality in the context of dynamical numerics applications. Namely, in the assessment of the mesh quality the common view is that the dihedral angle between the tetrahedron faces is a significant parameter determining the mesh quality−for the ideal mesh the measure of the dihedral angle between any faces should be $70.53°$. Therefore, the Stellar package is oriented mainly towards improving that parameter The simulations presented in this paper indicate, however, that at least for the diffusive-reactive model the improvement of the parameter connected with the quality of dihedral is not of a great importance−compare the results for Mesh 2 and Mesh 3 in Table 11. Apart from the fact that after applying Stellar package the dihedral angle parameter of the Mesh 3 is significantly better than that of Mesh 2−Table 9−the results for the both meshes are practically the same.

10. Concluding Remarks

As it has been aforementioned in Introduction, the main objective of this paper was to discuss the specifics of the quality measures of the generated mesh with respect to numerical calculations and fidelity of simulations. The obtained results lead to the following conclusions.

1. In the situation similar to that considered in this paper, the low quality mesh may alter the results of numerical simulations by a factor greater than two. In the context of modeling transmission of signals in the synapse such a low-fidelity result makes the simulation useless.
2. In the contrary to opinions expressed in a few papers, the dihedral angle in the case of our simulations did not prove an important parameter determining the quality of the simulation in the considered case.

The problem of generating the three-dimensional mesh itself is not trivial [30,31]. If the geometry of the simulated object is relatively simple−in our example, a geosphere or a globe with regular internal structures (like the spherically-shaped domain of neurotransmitter supply)−then generation of a 3D mesh of the object does not cause radical problems. The tetrahedral mesh generator like TetGen can easily produce a mesh of a satisfying quality (Tables 2, 4, and Figure 1). On the other hand, if the geometry of the model is complex, then generation of the mesh is faced with essential difficulties. Even such dedicated software as TetGen is not always capable of dealing with the problem. The quality of the created mesh is significantly worse (see Table 7 as well as Figures 10–12). However, even moderately optimized meshes seem to produce satisfying results.

References

1. Tadeusiewicz, R. New trends in neurocybernetics. *Comput. Methods Mater. Sci.* **2010**, *10*, 1–7.
2. Rama, S.; Zbili, M.; Debanne, D. Modulation of spike-evoked synaptic transmission: The role of presynaptic calcium and potassium channels. *Biochim. Biophys. Acta* **2015**, *1853*, 1933–1939. [CrossRef] [PubMed]
3. Zbili, M.; Rama, S.; Debanne, D. Dynamic control of neurotransmitter release by presynaptic potential. *Front. Cell. Neurosci.* **2016**, *10*, 278:1–278:24. [CrossRef] [PubMed]
4. Nanou, E.; Catterall, W.A. Calcium Channels, Synaptic Plasticity, and Neuropsychiatric Disease. *Neuron* **2018**, *98*, 466–481. [CrossRef] [PubMed]
5. Aristizabal, F.; Glavinovic, M.I. Simulation and parameter estimation of dynamics of synaptic depression. *Biol. Cybernet.* **2004**, *90*, 3–18. [CrossRef] [PubMed]
6. Bielecki, A.; Kalita, P. Dynamical properties of the reaction-diffusion type model of fast synaptic transport. *J. Math. Anal. Appl.* **2012**, *393*, 329–340. [CrossRef]
7. Bui, L.; Glavinovic, M. Temperature dependence of vesicular dynamics at excitatory synapses of rat hippocampus. *Cognit. Neurodynam.* **2014**, *8*, 277–286. [CrossRef]
8. Bielecki, A.; Kalita, P. Model of neurotransmitter fast transport in axon terminal of presynaptic neuron. *J. Math. Biol.* **2008**, *56*, 559–576. [CrossRef] [PubMed]
9. Friedman, A.; Craciun, G. A model of intracellular transport of particles in an axon. *J. Math. Biol.* **2005**, *51*, 217–246. [CrossRef] [PubMed]
10. Knödel, M.M.; Geiger, R.; Ge, L.; Bucher, D.; Grillo, A.; Wittum, G.; Schuster, C.; Queisser, G. Synaptic bouton properties are tuned to best fit the prevailing firing pattern. *Front. Comput. Neurosci.* **2014**, *8*, 101. [CrossRef]
11. Bielecki, A.; Kalita, P.; Lewandowski, M.; Siwek, B. Numerical simulation for a neurotransmitter transport model in the axon terminal of a presynaptic neuron. *Biol. Cybernet.* **2010**, *102*, 489–502. [CrossRef]
12. Bielecki, A.; Kalita, P.; Lewandowski, M.; Skomorowski, M. Compartment model of neuropeptide synaptic transport with impulse control. *Biol. Cybernet.* **2008**, *99*, 443–458. [CrossRef]
13. Lobos, C.; González, E. Mixed-element Octree: A meshing technique toward fast and real-time simulations in biomedical applications. *Int. J. Num. Methods Biomed. Eng.* **2015**, *31*, e02725:1–e02725:24. [CrossRef] [PubMed]
14. Yu, Z.; Holst, M.J.; McCammon, J.A. High-fidelity geometric modeling for biomedical applications. *Finite Elem. Anal. Des.* **2008**, *44*, 715–723. [CrossRef]
15. Yu, Z.; Wang, J.; Gao, Z.; Xu, M.; Hoshijima, M. New software developments for quality mesh generation and optimization from biomedical imaging data. *Comput. Methods Programs Biomed.* **2014**, *113*, 226–240. [CrossRef] [PubMed]
16. Wang, B.; Sun, Y.; Xu, N.; Mei, G. A Clustering-Based Bubble Method for Generating High-Quality Tetrahedral Meshes of Geological Models (Technical Note). *Appl. Sci.* **2020**, *10*, 5292. [CrossRef]
17. Liu, T.; Bai, S.; Tu, B.; Chen, M.; Lu, B. Membrane-channel protein system mesh construction for finite element simulations. *Mol. Based Math. Biol.* **2015**, *3*, 128–139. [CrossRef]
18. Gierdziewicz, M. Mesh geometric parameters for modeling signal transmission in the presynaptic bouton. *Lect. Notes Comput. Sci.* **2020**, *12415*, 1–12. [CrossRef]
19. Bielecki, A.; Gierdziewicz, M.; Kalita, P. A study on efficiency of 3D partial differential diffusive model of presynaptic processes. *Biocybernet. Biomed. Eng.* **2020**, *40*, 100–118. [CrossRef]
20. Bielecki, A.; Gierdziewicz, M.; Kalita, P.; Szostek, K. Construction of a 3D geometric model of a presynaptic bouton for use in modeling of neurotransmitter flow. *Lect. Notes Comput. Sci.* **2016**, *9972*, 377–386.
21. Bielecki, A.; Gierdziewicz, M.; Kalita, P. Three-dimensional model of signal processing in the presynaptic bouton of the neuron. *Lect. Notes Artif. Intell.* **2018**, *10841*, 3–14.
22. Bielecki, A.; Gierdziewicz, M. Simulation of neurotransmitter flow in three dimensional model of presynaptic bouton. *Lect. Notes Comput. Sci.* **2020**, *12139*, 132–143. [CrossRef]
23. Shewchuk, J.R. Delaunay Refinement Algorithms for Triangular Mesh Generation. *Comput. Geom.* **2002**, *22*, 21–74. [CrossRef]
24. Ciarlet, P.G. *The Finite Element Method for Elliptic Problems*; O'Malley, R.E., Jr., Ed.; Society for Industrial and Applied Mathematics: Philadelphia, PA, USA, 2002; pp. 110–143.

25. Si, H. *A Quality Tetrahedral Mesh Generator and 3D Delaunay Triangulator*; Version 1.5; User Manual; Weierstrass Institute for Applied Analysis and Stochastics (WIAS): Berlin, Germany, 2006. Available online: http://wias-berlin.de/software/tetgen/1.5/doc/manual/manual.pdf (accessed on 8 December 2020).

26. Si, H. TetGen, a Delaunay-based quality tetrahedral mesh generator. *ACM Trans. Math. Softw.* **2015**, *41*, 11:1–11:36. [CrossRef]

27. Shewchuk, J.R. What Is a Good Linear Element? Interpolation, Conditioning, and Quality Measure. In Proceedings of the 11th International Meshing Roundtable (IMC 2002), Ithaca, NY, USA, 15–18 September 2002; pp. 115–126.

28. Wilhelm, B.G.; Mandad, S.; Truckenbrodt, S.; Kröhnert, K.; Schäfer, C.; Rammner, B.; Koo, S.J.; Claßen, G.A.; Krauss, M.; Haucke, V.; et al. Composition of isolated synaptic boutons reveals the amounts of vesicle trafficking proteins. *Science* **2014**, *344*, 1023–1028. [CrossRef]

29. Klingner, B. Tetrahedral Mesh Improvement. Ph.D. Thesis, Department of Electrical Engineering and Computer Sciences, University of California at Berkeley, Berkeley, CA, USA, 2009.

30. Shewchuk, J.R. Tetrahedral mesh generation by Delaunay refinement. In Proceedings of the 14th Annual ACM Symposium on Computational Geometry (SCG 1998), Minneapolis, MN, USA, 7–10 June 1998; pp. 86–95. [CrossRef]

31. Zhou, Y.; Zhang, C.; Bo, P. Efficient tetrahedral mesh generation based on sampling optimization. *Comput. Animat. Virtual Worlds* **2015**, *26*, 577–588. [CrossRef]